Available online at www.sciencedirect.com

ScienceDirect

Procedia Manufacturing 47 (2020) 43–50

Procedia MANUFACTURING

www.elsevier.com/locate/procedia

23rd International Conference on Material Forming (ESAFORM 2020)

Influence of Simulation Parameters in the Combined Loading Compression Testing of CFRP Specimens

Maria Pia Falaschetti[a,*], Francesco Rondina[a], Lorenzo Donati[a], Enrico Troiani[a]

[a]*University of Bologna, DIN Department of Industrial Engineering, Viale Risorgimento 2, 40136 - Bologna, Italy*

* Corresponding author. Tel.: +39 054339774421. *E-mail address:* mariapi.falaschetti2@unibo.it

Abstract

In this paper a sensitivity study of a FEM model representing a carbon/epoxy composite material tested in Combined Loading Compression (CLC) is presented and the results are compared to experimental results. The present study aims to simulate the failure of composite materials when subjected to compression and crush loading conditions. This is required as a first step of a Building-Block Approach towards full-scale modelling of complex structures.
In the experimental part of the work, a laminate panel was manufactured with carbon unidirectional prepreg (Deltapreg UTS-300-DT120-37EF) in a cross-ply, balanced and symmetric stacking sequence, cured in autoclave at 120°C and 5 bar for 90 min. A number of six samples, extracted from the panel, were tested in compression following ASTM D6641/D6641M-16.
Numerical simulations have been implemented by means of the commercial software, ESI-VPS PAM CRASH. Boundary conditions, specimens' dimensions and material properties emulated real test conditions. A sensitivity study was performed on critical simulation parameters: the effect of mesh size and number of shell surfaces representing the composite stacking sequence was initially investigated. Furthermore, the specimen failure mode was inspected by the application of TIED links between the composite plies. Numerical results have been compared with experimental data and the comparison provided references for testing scale-up in the Building-Block Approach.

Keywords: composite materials; CFRP; numerical analysis; compression tests; CLC

Nomenclature

σ_{max}	Maximum Stress
E_{12t}	Young tensile longitudinal modulus
E_{23t}	Young tensile transverse modulus
G_{12}	Shear longitudinal modulus
E_{12c}	Young compressive longitudinal modulus
ν_{12}	Poisson modulus
G_{It}	Fracture energy mode I (tension)
G_{Ic}	Fracture energy mode I (compression)
G_{IIt}	Fracture energy mode II (tension)
G_{IIc}	Fracture energy mode II (compression)
G_{II12}	Fracture energy mode II (in plane shear)
E_{mean}	Average Young modulus
E_0	Young modulus
G_0	Shear modulus
τ_{max}	Maximum Shear strength
G_I	Fracture energy mode I
G_{II}	Fracture energy mode II
σ_{dt11}	Initial tensile stress damage limit (longitudinal dir.)
σ_{dc11}	Initial compressive stress damage limit (long. dir.)
σ_{dt22}	Initial tensile stress damage limit (transversal dir.)
σ_{dc22}	Initial compressive stress damage limit (trans. dir.)
σ_{d12}	Initial in-plane shear stress damage limit

1. Introduction

In the last thirty years, the use of composite materials increased significantly; in peculiar applications as well as in

2351-9789
10.1016/j.promfg.2020.04.119

everyday life, composite materials represent an improvement due to their properties-to-weight ratio.

Unfortunately, there still are many unknowns related to composite behaviour under several loading conditions and environments, in particular if specific requirements are set in the failure mode and post-failure behaviour. This leads too often to a not optimized use of these materials and to an unsuccessful exploiting of their advantageous properties. This is particularly true in the aeronautic field: for composite structures, aeronautical legislations still require high safety factors, able to satisfy no-growth principle. In order to cover these unknowns, experimental, numerical and analytical research studies are still running.

Nowadays numerical analyses for simulations of composite materials are widely used, thanks to many improvements in modelling and solving approaches. Finite Element Method (FEM) software has been widely developed, leading to a reliable implementation of materials' physical characteristics and behaviour.

Moreover, experimental tests campaigns require equipment, infrastructures and longer execution time, and consequently higher costs, than a numerical simulation. On the other hand, numerical simulations are solved on discretised domains and using simplified analytical formulas; their accuracy and correspondence with reality is therefore strictly dependent on how the models are implemented, which criteria are used for solution and material characteristics data employed. Some of these are in common between all FEM solvers, others (e.g. material failure approaches) depend on used software.

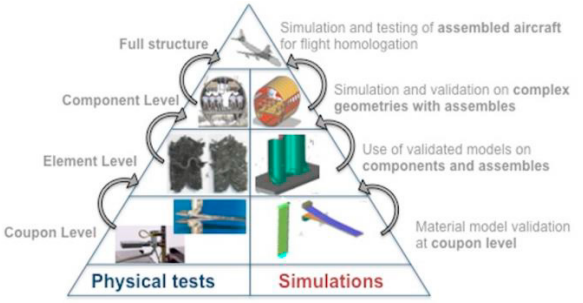

Fig. 1. The building block approach for aerospace sector.

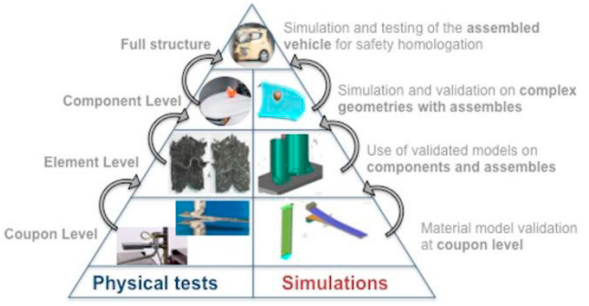

Fig. 2. The building block approach for automotive sector.

It is well known from the aerospace industry that composite structures are designed following the building block approach [1]. This methodology is usually represented by the pyramid concept reported in Fig. 1. The idea is to develop the knowledge on the material's structural behaviour and the validation of the simulation tools step by step, starting from the lower stage at the coupon level up to the full scale. The introduction of effective composite structures in primary parts of automotive vehicles follows the same approach (Fig. 2), in which the first stages of the pyramid are identical to the ones of Fig. 1 while specific applications only appear at the upper stages of the scale-up process. The engineers of the automotive industry are, therefore, facing the same problems as the aerospace engineers: they also need reliable predictive simulation tools for the development and homologation of the whole vehicle.

Moreover, the building block process cannot be run just once, but it has to be repeated every time the company decides to use different materials or to change simulations software.

In this paper a sensitive study on the first level of the pyramid (coupon level) was performed following Combined Loading Compression (CLC) tests (ASTM D6641/D6641M-16 [2-4]) by using the commercial software ESI-VPS PAM CRASH [5].

2. Experimental tests

Experimental campaign was conducted on a Carbon/Epoxy composite made by unidirectional prepreg (Deltapreg UTS-300-DT120-37EF), with a cross-ply, balanced and symmetric stacking sequence $[90/0_2/90/\overline{90}]_s$ followed by an autoclave curing cycle at 120°C and 5 bar for 90 min. Six samples were extracted from the laminate [6] and tested under compression in accordance with ASTM D6641-D6641M-16 [4] as described in [7].

Coupon dimensions are presented in Fig. 3: 140 mm long, 30 mm wide and 2.7 mm thick. Gauge length after clamping is 12 mm.

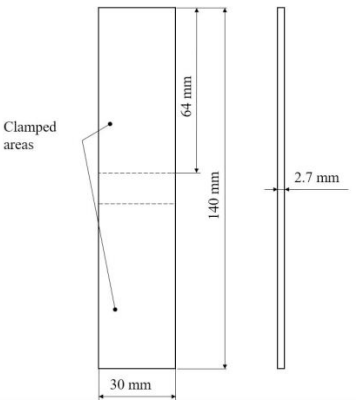

Fig. 3. Specimen geometrical dimensions

Specimens' designation and main results are summarized in Table 1. Young modulus (E_{mean} = 57.2GPa) was calculated equipping specimen A0 with two strain gauges (back-to-back configuration).

Ply data needed for implementation in the numerical model was obtained by means of other mechanical characterization tests, reported in [3]. Main material characteristics are listed in Table 2 to Table 4.

Table 1. Pristine coupons compression tests results

Specimen	Maximum load [kN]	σ_{max} [MPa]
A0	-33.35	-383.0
A1	-34.17	-416.6
A2	-32.85	-373.5
A3	-34.22	-391.9
A4	-32.59	-379.6
A5	-31.09	-370.1
Mean	-33.04	-385.8
St. Dev. [MPa]	1.17	16.9
CV [%]	3.5	4.4

Table 2. Deltapreg UTS-300-DT120-37EF properties (1)

E_{12t} [GPa]	E_{23t} [GPa]	G_{12} [GPa]	E_{12c} [GPa]	ν_{12} []
135.5	14.5	4.95	87	0.316

Table 3. Deltapreg UTS-300-DT120-37EF properties (2)

G_{It} [N/mm]	G_{Ic} [N/mm]	G_{IIt} [N/mm]	G_{IIc} [N/mm]	G_{II12} [N/mm]
107.5	48	0.47	1.79	1.79

Table 4. Deltapreg UTS-300-DT120-37EF properties (3)

σ_{dt11} [GPa]	σ_{dc11} [GPa]	σ_{dt22} [GPa]	σ_{dc22} [GPa]	σ_{d12} [GPa]
1.8	0.82	0.036	0.185	0.075

Moreover, experimental tests [3,5,11] were performed in order to obtain proper epoxy resin data which were implemented into numerical models simulating interlaminar layers (Table 5).

Table 5. Epoxy resin properties

E_0 [GPa]	G_0 [GPa]	σ_{max} [MPa]	τ_{max} [MPa]	G_I [N/mm]	G_{II} [N/mm]
14.5	4.95	36	43.5	0.47	1.79

3. Numerical model

Numerical simulations were performed using explicit ESI-VPS PAM Crash. This software, especially used in dynamic simulations [12-13], has good reliability on quasi-static simulation as well.

In order to reduce computational expenses, a simplified modelling approach was chosen: CLC fixture was modelled by means of proper boundary conditions applied on external coupons faces instead of implementing the whole fixture geometry. Four node two-dimensional elements were used to model laminate plies. In stacked-shell models, layers are tied at the ply interfaces, using two-node one-dimensional TIED elements to represent the mechanical characteristics of the resin rich interface. Material orientations follow specimen longitudinal (0° ply) and transversal (90° ply) directions. Load is applied along longitudinal direction.

The code uses the Waas-Pineda damage model [5,8-10] for element elimination. The model is based on damage initiation and propagation, the first set is equivalent to the failure envelope of the laminate. Damage propagation follows a cohesive-like formulation and is determined by the fracture energy of the particular failure mode. The model requires 5 inputs for the in-plane properties: fibre tension and compression, matrix tension, compression and shear as reported in Table 2 to Table 4. The model does not perform properly on single element simulations, because a bilinear behaviour is always imposed when the failure threshold is reached, as prescribed.

4. Parametric studies

Many parameters could influence FEA model results. The aim of this work is understanding which of chosen parameter is more effective on computational expenses and test results.

Investigated parameters were number of shell layers, mesh elements dimensions, element elimination criterion, load conditions and boundary conditions.

4.1. Number of shell parts

Specimens' stacking sequence was, as previously said, composed by 9 UD layers $[90/0_2/90/\overline{90}]_s$ resulting in a cured average thickness of 2.7 mm. Due to laminate thinness, authors took the opportunity to investigate two different approaches: modelling the whole stacking sequence into a single shell layer and modelling each ply as an individual layer. Using the first approach, on one hand, computational expenses are low, and a good correspondence is expected; on the other hand, there is not the chance to observe specimen realistic failure. This drawback was overcome by implementing 9 plies: in this approach, model is a closer representation of real conditions. Hereafter, these kinds of model will be addressed as 1-shell and 9-shells.

4.2. Mesh elements

Numerical analysis is sensible to mesh size; main influences are related to maximum load, failure mode, results accuracy, computational expenses.

Different elements dimensions were investigated in this work: 1 mm, 2 mm and 3 mm in case of 1-shell models, 1 and 2 mm in 9-shells models. For 1-shell model, elements were 4309 (1 mm mesh), 1050 (2 mm mesh), 506 (3 mm mesh); in case of 9-shells models there were 38781 (1 mm mesh) and 9450 (2 mm mesh) elements.

4.3. Element elimination

Another investigated parameter is the element elimination criterion. This is based on the percentage of failed layers in the shell element following the Waas-Pineda damage model.

Different values of this parameter were tested for 1-shell models: 70%, 85% and 100% of laminate failure, while for 9-shells, only 100% value is investigated, since each shell is used to model one individual ply.

4.4. Load application

CLC loading conditions are peculiar due to the combination of end and shear load, simultaneously applied to the specimens. This combination is not constant during the test, due to geometrical deformations, friction application and distribution. In fact, shear load is transferred by means of clamp force on external specimen faces; this is set constant at the beginning of

the test using a torque wrench to clamp the specimen in-between CLC fixture parallelepipeds, but it can change during test due to specimen bulging as reaction to compression.

Therefore, it was chosen to not simulate the clamping force but only the displacement imposed on external faces of the specimen by means of CLC surfaces.

For 1-shell models, only end-loading was implemented (Fig. 4) while for 9-shells models both end-loading and combined loading were analysed (Fig. 5).

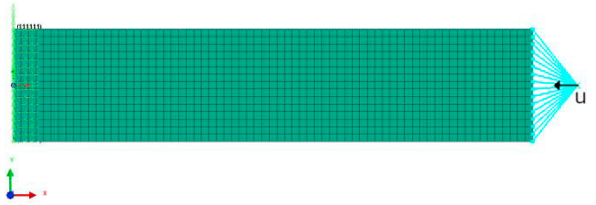

Fig. 4. 1-shell model: a constant displacement u is applied to the right-end nodes (cyan) while the left-end nodes (light green) are fixed.

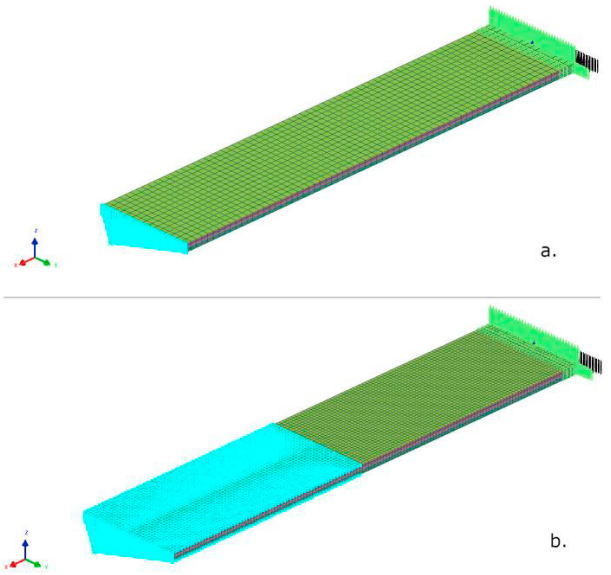

Fig. 5. 9-shells loading conditions: a. end load, b. combined load. In both cases, specimen fixed end is showed.

In fact, for 1-shell cases, imposing a displacement on the surface, simulating CLC shear loading, would have resulted in an improper boundary condition, neglecting inner layers movements. In 9-shells, shear load was applied on external plies (consequently transferred to other layers by TIED elements) while machine stroke was applied at one specimen free-end.

Load was introduced as a linear space-time history, simulating experimental tests conducted in displacement control. In order to reduce computational expenses, a higher velocity (130 mm/min) was chosen, applying a proper mass scaling in order to limit inertial effects.

In 9-shells, a comparison between higher and real test velocities was performed.

4.5. Boundary conditions

Different boundary conditions were needed depending on model settings, in particular with respect to loading application and shell parts number.

The still plate of the testing machine was implemented fixing one end of the specimen. A rigid body condition was used to link elements to an external node, where load was applied: in case of end-loading, only free-end elements, while, in case of combined load, elements on external faces and on free-end were involved.

CLC clamping surfaces were simulated limiting node movements in the affected areas. For 1-shell model all engaged nodes were forced to move only along loading direction; in the 9-shells models, this condition was applied to inner nodes (under fixture clamp area) while on the external faces no deformation was allowed.

In 9-shells, a self-contact condition between layers was needed, in order to avoid elements interpenetration during failure stages. It was achieved by means of contact type 36 in PAM Crash.

5. Results and discussion

5.1. Effect of element elimination and mesh size

In 1-shell models, three values of laminate failure percentage for element elimination were investigated: 70%, 85% and 100%. Fig. 6 displays maximum load results while Fig. 7 shows effect on computational expenses for all 1-shell models. It is possible to notice that element elimination settings have an imperceptible effect on maximum load while it affects more evidently CPU time.

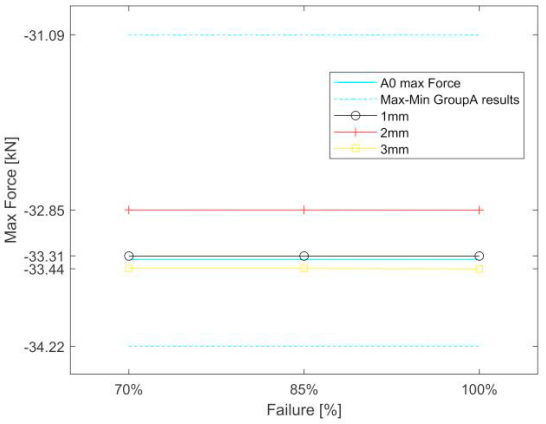

Fig. 6. Max force results: 1-shell models – comparison with specimen A0 and minimum and maximum values obtained for as-built coupons in experimental tests

As expected, computational time is higher as elements number rises, exceeding an hour in case of 1 mm mesh. Looking at different failure setups for the same mesh size, simulation time varies up to 20% between higher and lower value.

At the same time, maximum forces are slightly different: considering an experimental mean value of 33.04 kN, percentage error is +0.8%, +0.6% and -1.2% in case of 1 mm,

2 mm and 3 mm models respectively. Considering the maximum and minimum load value obtained in experimental tests (dotted lines in Fig. 6), numerical results are included inside the uncertainty range.

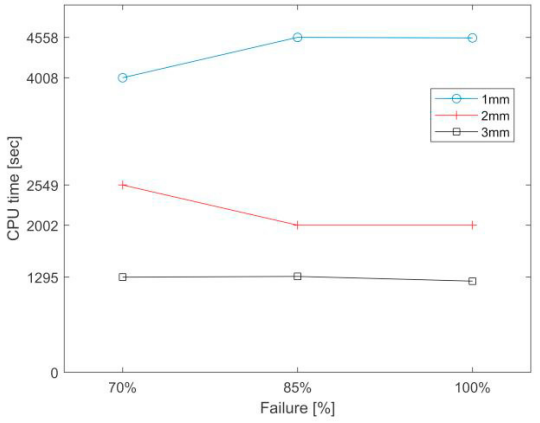

Fig. 7. CPU time results: 1mm-2mm-3mm mesh size models

In Fig. 8 to Fig. 10, experimental stress-strain curves are shown in comparison with numerical ones. Experimental plotted data are related to specimen A0 that was the only coupon equipped with strain-gauges. Both strain-gauges outputs, are presented. Authors underline the good congruity between 1 mm and 2 mm models with experimental material Young modulus: it is equal to 54.4 GPa and 54.2 GPa in the numerical simulations respectively (around 5% lower than experimental value). On the other hand, the 3 mm models were not able to capture the correct elastic modulus of the material: it is equal to 44.1 GPa resulting in a 23% error.

No evident effect of different element elimination setting can be seen. Each mesh size numerical models show same behaviour regardless of this parameter.

Considering element elimination set at 100% of laminate failure, a comparison in stress-strain results, between the three investigated mesh sizes, is presented in Fig. 11.

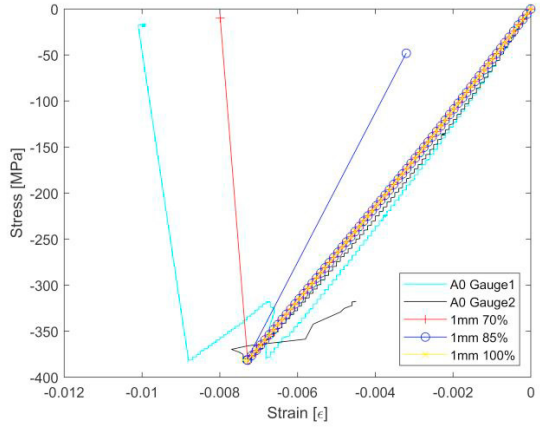

Fig. 8. Numerical-Experimental stress-strain results comparison 1-shell 1mm models

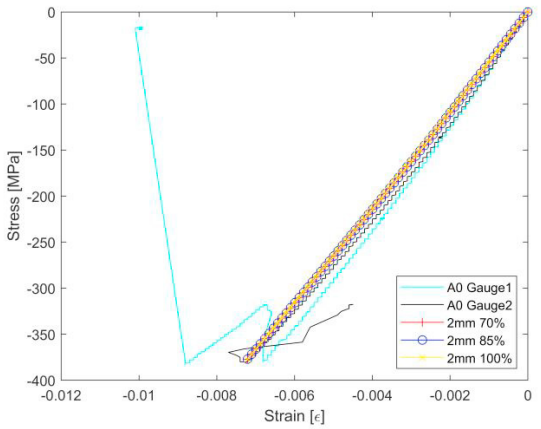

Fig. 9. Numerical-Experimental stress-strain results comparison 1-shell 2mm models

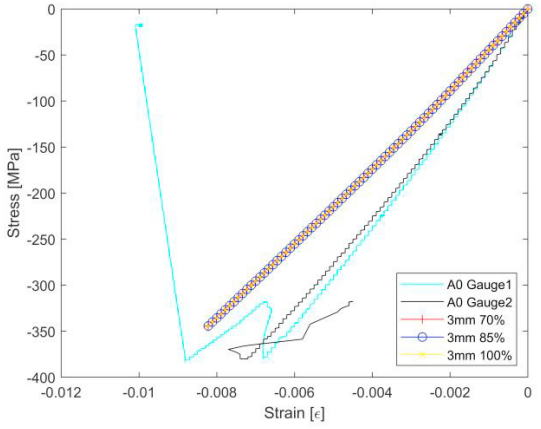

Fig. 10. Numerical-Experimental stress-strain results comparison 1-shell 3mm models

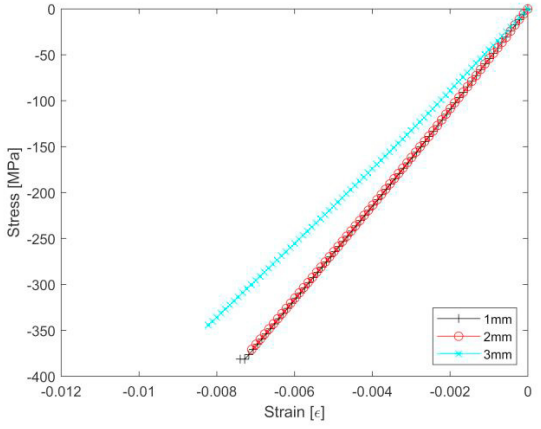

Fig. 11. Numerical stress-strain comparison results 1mm-2mm-3mm models (100% elements elimination)

Good agreement with experimental results (as previously highlighted) is showed in 1 mm and 2 mm models while a 3 mm model differs greatly.

In case of 9-shells, 3 mm model was dismissed. For comparison with 1-shell regarding mesh size, end load was applied.

Fig. 12 shows that both mesh sizes are in good agreement with experimental results: maximum force and Young modulus indicate an error of -0.6% and 5.2% respectively in both cases. Differences are evident in CPU time: it is equal to 17690 seconds for a 2 mm mesh, while it rises to 68030 seconds for the thinner mesh.

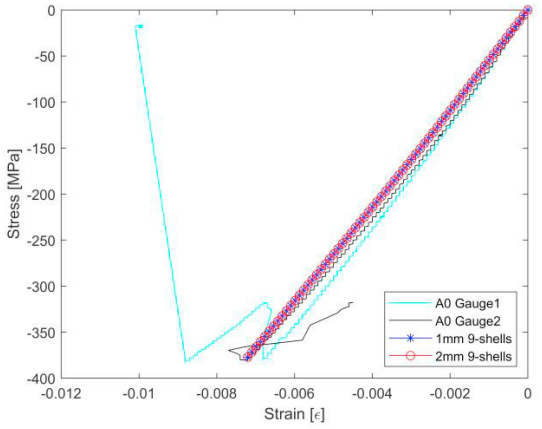

Fig. 12. Numerical-Experimental stress-strain results comparison 9-shells 1mm mesh and 9-shells 2mm mesh size models

5.2. Effect of load

In 9-shells models it was possible to test both end-loaded and CLC loading conditions. In Fig. 13 a comparison between 1 mm models with the two different loading conditions is presented. Models show a good agreement between each other, proving the good similarity of CLC results with other traditional compression test fixtures [2,4]. Moreover, a good agreement is displayed with experimental results, as well.

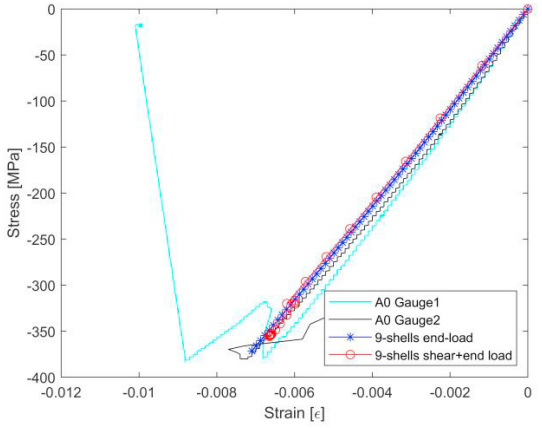

Fig. 13. Numerical-Experimental stress-strain results comparison of 9-shells models (end-loading and combined loading condition)

Testing velocity effect was analysed as well. A 1 mm elements 9-shells model, with combined compression loading, was used. Experimental test velocity (1.3 mm/min) and the higher one (130 mm/min, already used in previous simulations) were tested.

In the latter case, proper mass-scaling was implemented to limit dynamic inertial effect. Fig. 14 presents both numerical stress-strain curve results in comparison with experimental ones. On one hand, a good agreement is achieved in both cases; on the other hand, computational expenses are widely different: in case of increased speed, CPU time is equal to 17.3 hours, while for the real testing velocity, it rises to 1898.9 hours (79.1 days).

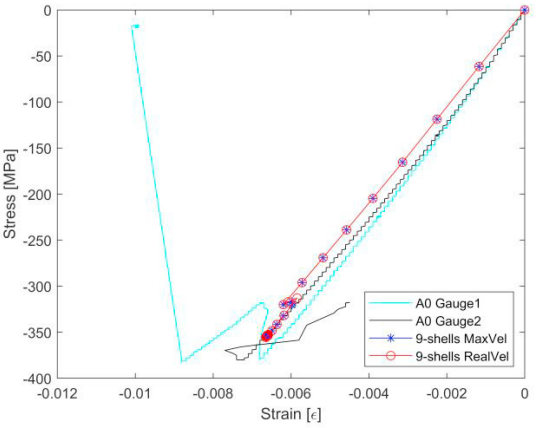

Fig. 14. Numerical-Experimental stress-strain results comparison of 9-shells models at different loading velocities

5.3. Effect of parts number

As previously said, computational time required for simulations is higher in case of 9-shells compared to 1-shell models. Due to good agreement with experimental tests in all 1 mm and 2 mm mesh models (as Fig. 15 displays), if only mechanical characteristics are needed, a simplified model is recommended. To obtain a representation of specimen failure mode, however, it is necessary to build up a more complete model with one shell per each ply.

In Fig. 16, laminate failure mode details, for end loaded 9-shells models, are presented. In both cases, specimens fail in the middle of gauge length due to layers local buckling.

Bigger mesh, however, results in a widespread damage, unable to portray the real coupon failure. The smaller mesh size shows an improvement, but failure behaviour is still different from real coupons' (Fig. 17).

Fig. 18 displays 1-shell failure for 1 mm and 2 mm mesh. In both cases, an entire row of elements disappears simultaneously, and no local buckling is highlighted.

Considering 9-shells combined loaded model, even though stress-strain results and nodes displacement pattern are in good accordance with experimental tests (Fig. 19), resulting failure mode is far from a realistic one. TIED layers, linking external plies to the inner ones, fail prematurely, due to shear load. This kind of failure was not observed in experimental tests. A possible reason could be an improper resistance of TIED elements to this kind of load.

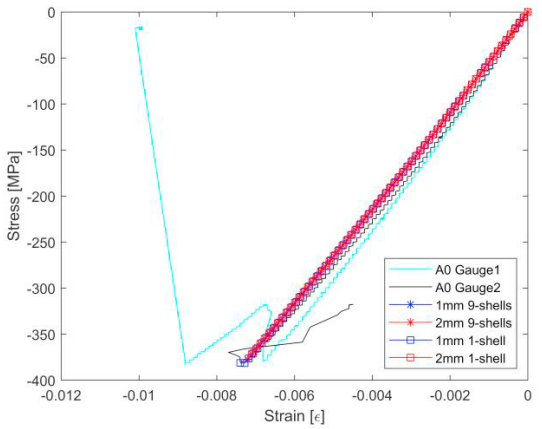

Fig. 15. Numerical-Experimental stress-strain results comparison of 1-shell and 9-shells models with 1 mm and 2 mm mesh size

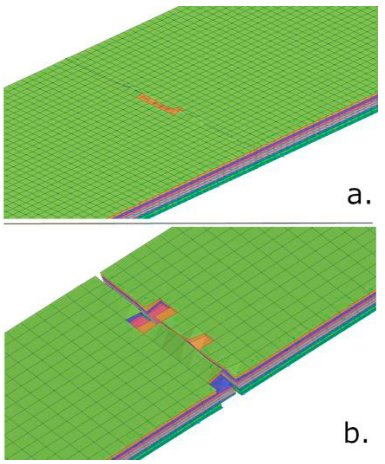

Fig. 16. 9-shells 1mm model: Failure detail (no contour displayed) – a. 1mm model, b. 2mm model

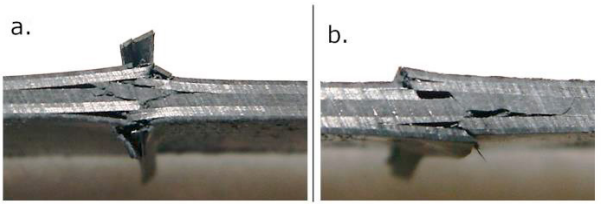

Fig. 17. Experimental failure examples: a. BGT, b. HGM (failure modes classified as described in [4])

An attempt to overcome this numerical issue, was performed: a 3D element layer was inserted between outer layers and first TIED layer (Fig. 20) [14-15]. The aim was to apply a smoother distribution of the shear load component. Results showed that TIED elements still fail prematurely, even if few moments later than in the case without the solid layer; specimen failure takes place due to external plies local buckling (Fig. 21).

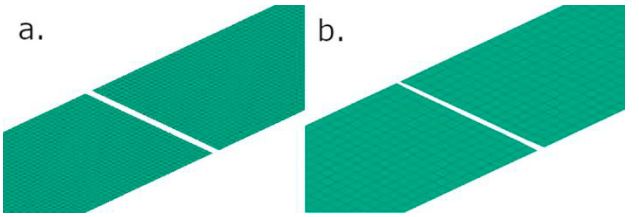

Fig. 18. 1-shell Failure detail (no contour displayed) - a.1mm model, b. 2mm model

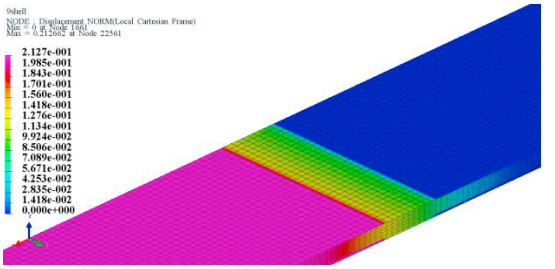

Fig. 19. 9-shells 1mm model: displacement along loading direction contour

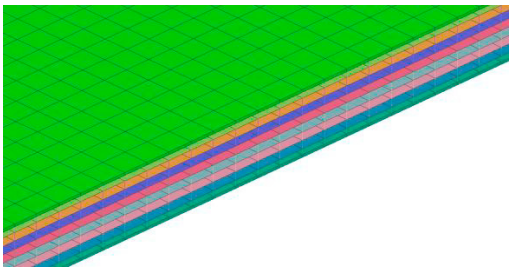

Fig. 20. 9-shells 1mm model: detail on solid elements resin layer

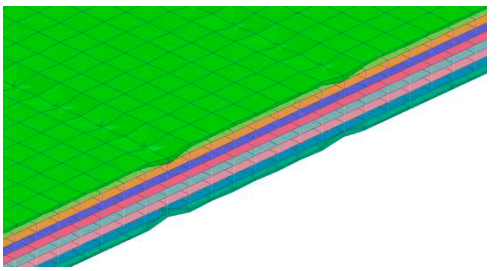

Fig. 21. 9-shells 1mm model: solid elements resin layer, detail on failure (no contour displayed)

In addition, even in 9-shells end loaded models, it is not fully highlighted the 'brooming' failure that specimens typically show in experimental compressive tests [2,4,7]. This could be due to the complex post-failure nature of this damage mode which generates a 3D stress state, not possible to capture with shell elements. Solid elements could overtake this task.

6. Conclusions

In this paper, experimental compression tests on a carbon/epoxy laminate was reproduced by means of a Finite Element Method modelling. Explicit ESI-VPS PAM Crash was used. Some numerical parameters were investigated: layer

numbers, mesh size, element elimination settings, and loading conditions.

In order to compare different element elimination setups, models with just one shell layer, portraying the whole laminate stacking sequence, were implemented. Failure percentages equal to 70%, 85% and 100% were investigated at different mesh sizes (1, 2 and 3 mm). Results proved that computational time was more affected by mesh sizes than element elimination as well as maximum force. Moreover, it was proved that 3 mm mesh size is not suitable to obtain reliable laminate mechanical characteristics: error related to Young moduli was about 23% while for a 2 mm model it was about 5%.

End-loading and combined loading were tested in 9-shells models. These simulations resulted in good agreement with experimental tests, both in force and Young modulus, proving the reliability of the CLC test fixture in testing composite materials in compression.

Both real and higher loading velocity were simulated in combined case. Good results were obtained in both cases; however, computational expenses were quite high for modelling real testing velocity: CPU time was 79.1 days.

In order to reproduce laminate failure mode, models with one shell per each carbon/epoxy ply, were run. 1 mm and 2 mm mesh sizes were tested in this case. The first one, in case of end loaded model, showed a better but still far from a realistic failure representation.

Combined loading models, even though in good agreement with stress-strain experimental results, resulted in an unrealistic failure. To overcome this issue an attempt of modelling resin rich areas differently was made. Results showed a slight improvement but did not represent thus far a close to reality failure. In order to obtain a better portrayal of specimen rupture, and 'brooming' peculiar mode, more numerical studies are needed.

Between analysed, the most effective parameter on mechanical characteristics was mesh size: 3-mm elements models resulted in a 23% error on Young modulus compared to a 5% in 1- and 2-mm ones. Unexpectedly, no effect was seen related to element elimination setting.

Considering computational expenses, the number of shell parts was the most compelling. Considering only the higher loading velocity, CPU time was in the range of minutes for the 1-shell and of almost one day for the 9-shells.

Acknowledgements

Authors thank ENEA Laboratory of Materials Technologies Faenza (TEMAF) for the experimental support.

References

[1] Bruyneel M, Naito T, Urushiyama Y, McDougall S. Predictive simulations of damage propagation in laminated composite materials and structures with LMS Samtech Samcef. SAE World Congress. 2015; 2015-01-15M-0352.

[2] Wegner PM, Adams DF. Verification of the Combined Load Compression (CLC) Test Method. FAA Final Report DOT/FAA/AR-00/26; 2000.

[3] MIL-HDBK-17-1F – Composite Materials Handbook, Volume 1, Polymer Matrix Composites Guidelines for Characterization of Structural Materials. 2002

[4] ASTM D6641/D6641 M-16 - Standard Test Method for Compressive Properties of Polymer Matrix Composite Materials Using a Combined Loading Compression (CLC) Test Fixture. 2016.

[5] ESI Visual PAM-Crash 13.0 user's manual

[6] ASTM D 5687/D 5687 M-95 – Standard Guide for Preparation of Flat Composite Panels with Processing Guidelines for Specimen Preparation. Reapproved 2007.

[7] Falaschetti MP, Scafè M, Troiani E, Agostinelli V, Sangiorgi S. Experimental Determination of Compressive Residual Strength of a Carbon/epoxy Laminate after a Near-edge Impact. Procedia Engineering. 2015; 109:171-80.

[8] Pineda EJ, Waas AM, Bednarcyk BA, Collier CS, Yarrington PW. A Multiscale Progressive Damage and Failure Modeling Approach For Laminated Fiber Reinforced Composites. Advances in Mathematical Modeling and Experimental Methods for Materials and Structures. Solid Mechanics and Its Applications. 2009; 168:43-56.

[9] Pineda EJ, Waas AM, Bednarcyk BA, Collier CS. Multiscale Model for Progressive Damage and Failure of Laminated Composites Using an Explicit Finite Element Method. 50th AIAA/ASME/ASCE/AHS/ASC Structures, Structural Dynamics, and Materials Conference. 2009. Palm Springs, California.

[10] Pineda EJ, Waas AM. Modelling progressive failure of fibre reinforced laminated composites: mesh objective calculations. The Aeronautical Journal. 2012;116(1186):1221-46.

[11] Camponeschi E. Compression of Composite Materials: A Review, in Composite Materials: Fatigue and Fracture (Third Volume). ASTM International. 1991; p.550-78.

[12] Greve L, Pickett AK. Delamination testing and modelling for composite crash simulation. Composites Science and Technology. 2006; 66(6):816-26.

[13] Solanki K, Oglesby D, Burton C, Fang H et al. Crashworthiness Simulations Comparing PAM-CRASH and LS-DYNA. SAE Technical Paper 2004-01-1174. 2004.

[14] Krueger R, Shivakumar K, Raju I. Fracture mechanics analyses for interface crack problems - A review. 54th AIAA/ASME/ASCE/AHS/ASC Structures, Structural Dynamics, and Materials Conference. 2013. Boston, Massachusetts.

[15] Raju I, Crews J, Aminpour M. Convergence of strain energy release rate components for Edge-Delaminated composite laminates. Engineering Fracture Mechanics. 1988; 30 (3): 383-96.